IOPscience iopscience.iop.org

Home Search Collections Journals About Contact us My IOPscience

Structural and Mössbauer spectral study of the metastable phase $Sm(Fe, Co, Ti)_{10}$

This article has been downloaded from IOPscience. Please scroll down to see the full text article.

2002 J. Phys.: Condens. Matter 14 8111

(http://iopscience.iop.org/0953-8984/14/34/329)

View the table of contents for this issue, or go to the journal homepage for more

Download details:
IP Address: 171.66.16.96
The article was downloaded on 18/05/2010 at 12:28

Please note that terms and conditions apply.

INSTITUTE OF PHYSICS PUBLISHING JOURNAL OF PHYSICS: CONDENSED MATTER

J. Phys.: Condens. Matter **14** (2002) 8111–8120 PII: S0953-8984(02)36472-5

Structural and Mössbauer spectral study of the metastable phase Sm(Fe, Co, Ti)$_{10}$

L Bessais[1,3], **C Djéga-Mariadassou**[1] **and E Koch**[2]

[1] LCMTR, UPR209, CNRS, 2/8 rue Henri Dunant, BP 28 F-94320 Thiais, France
[2] Institut für Mineralogie, Petrologie und Kristallographie, Philipps-Universität Marburg Hans-Meerwein-Straße, D-35032 Marburg, Germany

E-mail: bessais@glvt-cnrs.fr

Received 1 May 2002
Published 15 August 2002
Online at stacks.iop.org/JPhysCM/14/8111

Abstract

We have performed a Mössbauer spectral analysis of nanocrystalline metastable $P6/mmm$ SmTi(Fe$_{1-x}$Co$_x$)$_9$, correlated with structural transformation towards its equilibrium derivative $I4/mmm$ SmTi(Fe$_{1-x}$Co$_x$)$_{11}$. The Rietveld analysis shows that the 3g site is fully occupied, while the 6ℓ occupation is limited to hexagons surrounding the Fe–Fe dumb-bell pairs 2e. A specific programme for the Wigner–Seitz cell (WSC) calculation of the metastable disordered structure was used. The hyperfine parameter assignment based on the isomer shift correlation with the WSC volumes sequence leads to Co 3g preferential occupation, with Ti location in 6ℓ sites. The mean hyperfine field increases with Co content in connection with the enhancement of the negative core electron polarization term upon additional Co electron filling. The same trend is observed for each individual site leading to the sequence $H_{HF}\{2e\} > H_{HF}\{6\ell\} > H_{HF}\{3g\}$.

1. Introduction

A metastable phase is not the most thermodynamically stable phase, but a temporarily stable one under certain conditions. The metastable phase forms under conditions corresponding to a local minimum of the free energy. These phases have been investigated extensively for the last two decades, as the formation of metastable phases opens a new way of searching for novel permanent-magnet materials. One of the motivations for the investigations is their outstanding magnetic properties which are important for practical applications. Furthermore, the study of the formation of metastable phases and their transformation into the various equilibrium phases is most important for achieving a better understanding of the relation between crystal structure and intermetallic thermodynamic stability.

[3] Author to whom any correspondence should be addressed.

 © 2002 IOP Publishing Ltd Printed in the UK

Various processes can be used to prepare metastable phases. The most convenient method is first to reach the amorphous phase and then to anneal it at an appropriate temperature. The main paths to the amorphous state are mechanical alloying, rapid quenching, and the processes of hydrogenation, disproportionation, desorption, and recombination (HDDR). Mechanical alloying, i.e. high-energy ball milling and subsequent annealing of the as-milled powders, has been found to improve the solid-state reaction. The amorphization achieved by mechanical alloying is due to mechanically induced disorder and microstructural refinements. It involves reducing the grain size to a critical value, disorder and defects introduced during milling, and a solid-state amorphization reaction between adjacent layers welded together during milling.

The basic aim of research into permanent-magnet materials is to combine an inexpensive transition metal, with a high Curie temperature and high magnetization, with another element, such as a rare earth, in such a way that the resulting compound has high uniaxial magnetic anisotropy. The large-scale size difference between the rare earth and the transition metal gives rise to the observation of many anisotropic crystal structures. In such systems the transition metal (T) is responsible for most of the magnetization and T–T exchange determines the Curie temperature. On the other hand, the rare earth (R) determines the magnetocrystalline anisotropy. The anisotropic 4f-electron charge densities on the rare-earth ion give rise to a large orbital moment and consequently large spin–orbit interactions that are at the root of magnetocrystalline anisotropy. The development of large coercivities from materials with large (uniaxial) magnetic anisotropies involves microstructural impediments intended to supply barriers to the rotation of the magnetization and pinning of domain walls.

Amongst the new rare-earth–transition-metal (R–T) hard magnetic materials with a stable or metastable structure, in particular Sm-containing iron-rich intermetallic compounds have been considered as potential candidates for permanent-magnet application—such as $SmFe_{11}Ti$ and $Sm_2Fe_{17}N_3$ [1, 2].

Using a conventional melting technique, Ray [3] and Buschow [4] discovered the existence of a number of equilibrium intermetallics R_2T_{17} which were shown to crystallize in the $R\bar{3}m$ Th_2Zn_{17} type of structure. This structure can be derived from the well-known $CaCu_5$ structure, denoted as RT_5, by replacing a third of all atoms in a regular manner by pairs of smaller T–T atoms (dumb-bells). In the case of the Sm–Fe alloys, Ray gave originally the compositional formula $SmFe_7$ although no chemical analyses were performed on that compound. He found, however, that the lattice constants were consistent with the triple primitive cell RT_5.

Cadieu and co-workers [5, 6] found that the Sm–Fe compound with a $CaCu_5$-type structure can be stabilized by use of a third element, such as Ti, by means of selectivity thermalized sputtering. Besides the well-known equilibrium phases of the binary Sm–Fe system, in melt-spun ribbons of Sm–Fe a hexagonal $TbCu_7$-type $P6/mmm$ phase, a subcell of the Th_2Zn_{17} structure, has been demonstrated, by Katter *et al* [7]. The relative populations of the various atom species were deduced from the nominal composition $SmFe_9$, taking into account that the stoichiometry of the $TbCu_7$ structure could be written as $Sm_{1-s}Fe_{5+2s}$ with $s = 0.34$; s expresses the number of R substitutions. Previously, we had investigated [8] the emergence of order in nanocrystalline Sm–Fe alloys prepared by mechanical alloying. With this technique, the out-of-equilibrium precursor phases can be observed prior to the equilibrium phases, according to the annealing temperature of the as-milled powder. The out-of-equilibrium $SmFe_9$ compound was obtained with its composition deduced from Rietveld technique x-ray diagram analysis, in agreement with Teresiak [9], after annealing at low temperature ($T < 750\,^{\circ}C$). At high temperature the $R\bar{3}m$ phase occurs with composition Sm_2Fe_{17}.

The T-excess region of the RT_5 formula, described as $R_{1-s}T_{5+2s}$, can generate other well-known equilibrium structures when a third element T′ with adequate atomic radius and

electronic structure is involved. When two of five R atoms are replaced with dumb-bells in a regular way, the monoclinic $R_3(T, T')_{29}$ structure with space group $P2_1/c$ is obtained [10]. Furthermore, when two dumb-bell pairs (T–T) substitute for 2R atoms over a $4R(T, T')_5$-type cell, the tetragonal $R(T, T')_{12}$ $ThMn_{12}$ structure with space group $I4/mmm$ is formed [11, 12].

In this contribution, we focus our attention on the structure and the Mössbauer spectral analysis of the metastable precursors $SmTi(Fe_{1-x}Co_x)_9$ for low cobalt content, obtained by mechanical alloying.

2. Experiment

The samples were obtained by ball milling Fe (99.9 %), Co (99.9%), Ti (99.9%), and Sm (99.9%) powders under an Ar atmosphere for 5 h. The samples wrapped in tantalum foils were annealed in a sealed quartz tube under 10^{-6} Torr at temperatures between 600 and 850 °C for 30 min.

X-ray diffraction measurements were carried out with Cu Kα radiation on a Bruker diffractometer equipped with a single-crystal graphite monochromator. The data were fitted using the FULLPROF [13, 14] computer code based on Rietveld analysis [15, 16], which permits the refinement of each coexisting phase and takes into account the broadening of the diffraction lines induced by grain size and strain effects, with the assumption of a Thompson–Cox–Hastings line profile. The Curie temperatures T_C were measured on a differential sample magnetometer (MANICS) in a relatively low magnetic field of 1000 Oe.

^{57}Fe Mössbauer spectra were collected at room temperature using a constant-acceleration 512-channel spectrometer working in the mirror image mode. The α-iron reference had a full width at half-maximum of 0.25 mm s^{-1} for the external peaks. The spectra were classically least-squares fitted assuming Lorentzian lines. The estimated errors are ± 1 kOe for hyperfine fields (H_{HF}), and ± 0.005 mm s^{-1} for the isomer shifts (δ) and quadrupole interaction (2ϵ).

3. Results and discussion

3.1. Phase formation and structure

We have studied the magnetic properties correlated with the structural transformation from the metastable $P6/mmm$ hexagonal $CaCu_5$-type subcell to the $SmFe_{11}Ti$ $ThMn_{12}$ structure. The results of the Rietveld analysis of the primitive cell have given a samarium and transition metal Fe, Ti stoichiometry of 1:10, slightly different from that of the ordered recurrent 1:12 compound.

It appears that the precursor phase obtained via the out-of-equilibrium path does not correspond to the exact stoichiometry of its equilibrium limit, but to the closest composition consistent with the crystalline symmetry transformation.

The lattice parameters of the tetragonal $ThMn_{12}$-type phase can be converted into those of the hexagonal $CaCu_5$-type phase according to the following conversion equations: $a_{1:5} = c_{1:12}$ and $c_{1:5} = a_{1:12}/2$

The $CaCu_5$ is constituted by the R lattice built at the coordinate origin 1a (0, 0, 0) and 2T sublattices built on 2c ($\frac{1}{3}$, $\frac{2}{3}$, 0) and 3g ($\frac{1}{2}$, 0, $\frac{1}{2}$) positions. This arrangement leads to two types of layer: in the lowest one, R atoms are centred on T hexagons, whereas in the next layer, only T atoms are accommodated.

The Givord *et al* model [17] gives the possibility of taking into account the T distortion obviously brought about by the R substitution. Moreover, higher T enrichment gives evidence of the additional 6ℓ site, from the fact that only the 2c site cannot be used to describe such T

Table 1. The number of subsequent atoms in the various Wyckoff positions of the ordered $I4/mmm$ $ThMn_{12}$-type unit cell ($s = 0.5$) and the $P6/mmm$ $CaCu_5$-type subcell ($s = 0.42$). For comparison to the tetragonal cell R_2T_{24}, the last column gives the number of atoms for the four hexagonal subcells consistent with the RT_{10} formula.

	RT_{12}		RT_{10}		
Sm	2a	2	1a	$1 - s = 0.58$	2.32
Fe/Co	8f	8	3g	2	8
Fe	8j	8	3g	1	4
			6ℓ	1	4
Fe/Ti	8i	8	6ℓ	1	4
			2e	$2s = 0.84$	3.36
Total number		26			25.68

content. The more general 6ℓ $(x, 2x, 0; x \neq \frac{1}{3})$ site which relates to the previous 2c hexagons implies an atom occupation rate limited to $\frac{1}{3}$. At most one third of the 6ℓ T atoms forming the hexagon surround the dumb-bell 2e $(0, 0, z)$. For the RFeT′ (T′ = Ti, Co) compounds, the x-ray Rietveld technique allows an accurate determination only of the R content owing to the close atomic diffusion factor values of the Fe and T′ atoms. Therefore, one might have interpreted the x-ray diagrams with the assumption of a statistical distribution of Fe, Ti, Co. However, we have fitted the x-ray patterns according to the atomic distribution used for the interpretation of the Mössbauer spectra based on the relationship between $I4/mmm$ and $P6/mmm$ structures. Such mechanisms applied to the hexagonal precursor of the $ThMn_{12}$ $Sm(Fe,Co)_{12}Ti$ leads to three iron sites, 2e, 6ℓ, and 3g.

From table 1, one can note the relationship between the tetragonal equilibrium phase and its metastable hexagonal precursor. All of the 8f atoms occupy two thirds of the 3g sites. The 8j sites will be equally shared between the remaining third of the 3g sites and half of the 6ℓ sites. The 8i sites will transform into the other half of the 6ℓ sites and the 2e site, characterized by $2s$ atoms. The correlated samarium content is equal to $(1 - s)$.

The x-ray diagrams reveal unambiguously, for all samples, the hexagonal phase $P6/mmm$ as the main phase. Owing to the extreme care taken with the handling procedures—performed in a glove box with O_2 and H_2O levels around 1 ppm—the presence of a small amount of oxide can only be explained by nitrogen and oxygen traces still present in the initial powders (SmO–N, Sm_2O_3).

Moreover due to the nanoscale size of the samples, x-ray microprobe analysis could not be implemented specifically on the $CaCu_5$ domains. The phase stoichiometry has only been deduced from the Rietveld refinements.

The fitted value of s for the hexagonal precursor of $Sm_{1-s}(Fe,Ti,Co)_{5+2s}$, $SmTi(Fe_{1-x}Co_x)_9$, is found to be equal to 0.42 ± 0.01. The 1:12 composition has s equal to 0.5.

Consequently, the total number of atoms in the four hexagonal subcells is equal to 25.68, consistent with the RT_{10} formula. This hexagonal structure is over-stoichiometric in samarium with respect to the RT_{12} compounds (see table 1).

3.2. Wigner–Seitz cell volume calculation

We have based the Mössbauer spectral analysis upon two criteria:

(i) Counting of the different iron neighbours according to the binomial law (as described below).

Table 2. WSC-derived near-neighbour environments and volumes in $SmTiFe_9$, $P6/mmm$.

Site	Fe (2e)	Ti/Fe (6ℓ)	Fe (3g)	Iron near neighbours	WSV (Å^3)
Fe (2e)	1	6	6	11.32	17.06
Ti/Fe (6ℓ)	2	2	6	9.44	12.37
Fe (3g)	2	4	4	8.88	12.65

Table 3. Interatomic distances for the hexagonal $P6/mmm$ structure ($a = 4.899$ Å, $c = 4.225$ Å).

Site	Distance (Å)	Number of Fe atoms	Notation
6ℓ	2.44	1.44	6ℓ
	2.47	4	3g
	2.78	2	3g
	2.75	2	2e
2e	2.53	1	2e
	2.59	6	3g
	2.75	4.32	6ℓ
3g	2.45	4	3g
	2.47	2.88	6ℓ
	2.60	2	2e

(ii) Assignment of the hyperfine parameter sets, δ, H, and 2ϵ, of an individual sextet to its correct crystallographic site, in agreement with the relationship between the isomer shift and the Wigner–Seitz cell (WSC) volumes; the larger the WSC volume, the larger the isomer shift δ.

The WSC volumes have been calculated by means of Dirichlet domains and coordination polyhedra for each crystallographic family. We have used the procedure of radical planes, which results in a space partition without gaps between the polyhedra [18]. The radius values of 1.81, 1.26, and 1.47 Å have been used respectively for Sm, Fe, and Ti.

We have simulated the partial occupation by performing the calculations in an appropriate $P6/mmm$ subgroup in a way that allows the splitting of the partially Ti-occupied positions. The simplest possibility is given in subgroup $P1$ with $a' = 3a, b' = 3b, c' = c$, where we had to take into account all atoms corresponding to the fully occupied positions (20 atoms) and one additional atom from one of the other positions.

The WSC volumes resulting from such calculations (see table 2) lead to the following volume sequence: $V\{2e\} > V\{3g\} > V\{6\ell\}$, whatever the Co content.

To assign the Mössbauer components to each crystallographic site, nearest-neighbour environments were considered, and the results for a radius equal to 2.78 Å around each atom are shown in table 3.

3.3. Mössbauer spectral analysis

The Mössbauer spectra relating to the hexagonal phase obtained at room temperature, together with the fits, are shown in figure 1. We must point out that the atomic arrangements are rather complex due, on the one hand, to the existence of three crystallographic sites and, on the other hand, to the statistical distribution of titanium and cobalt. Consequently, the experimental spectra result from the convolution of numerous sextets. Various sets of hyperfine parameters

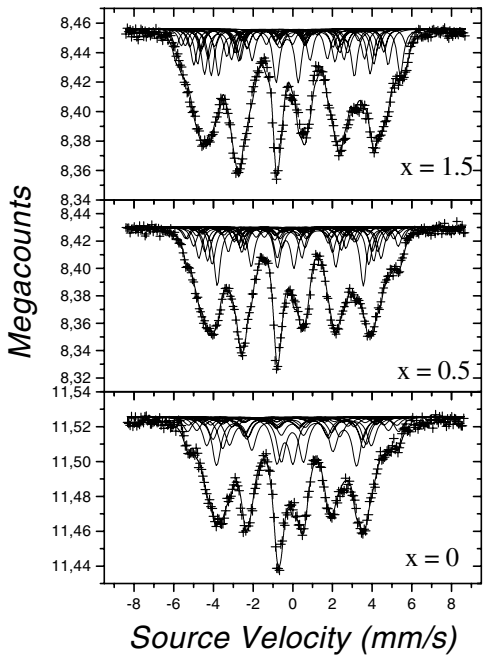

Figure 1. The 293 K Mössbauer spectra of $SmTi(Fe_{1-x}Co_x)_9$.

might lead to a good reproduction of the data but the choice of the solution is dependent upon consistent physical models supported by other techniques or justified by pertinent theoretical considerations.

Four assumptions have been made:

(i) Half of the 6ℓ sites are occupied statistically by titanium. The atomic radius of this element must be greater than the Fe radius and the number of its 3d–4s electrons is smaller [19]. The result is that the possibility of Co substitution at the 6ℓ site has been excluded.
(ii) Cobalt atoms occupy statistically two thirds of 3g sites.
(iii) The Lamb–Mössbauer factors were equal for all sites 2e, 3g, and 6ℓ of the $CaCu_5$ structure.
(iv) As no crystallographic texture was observed, the relative intensities of the sextet lines were taken to be in the ratio 3:2:1 of random powders.

Consequently, in the first step we calculated the relative abundances of the Fe families in the various crystallographic sites 2e, 3g, and 6ℓ with the assumption of titanium located in the 6ℓ site, cobalt in the 3g site, with a multinomial law as follows.

Let p_0 be the atomic proportion of the host iron atom in the alloys and p_k the atomic proportion of the kth alloying element; $\sum_{k=0}^{K} p_k = 1$.

As the atoms are distributed randomly among the spheres i with $i = 1, 2, 3$, the probability P_{α_i} of a given configuration $\alpha_i = \{n_{1,i}, \ldots, n_{k,i}\}$, with k varying from 1 to 6 for $i = 1$ (2e), 1 to 2 for $i = 2$ (6ℓ), and 1 to 4 for $i = 3$ (3g), follows the well-known multinomial distribution law:

$$P_{\alpha_i} = \frac{N_i!}{\prod_{k=0}^{K} n_{k,i}!} \prod_{k=0}^{K} p_k^{n_{k,i}} \tag{1}$$

where N_i is equal to 6, 2, and 4 for respectively $i = 1$, 2, and 3 (see table 2).

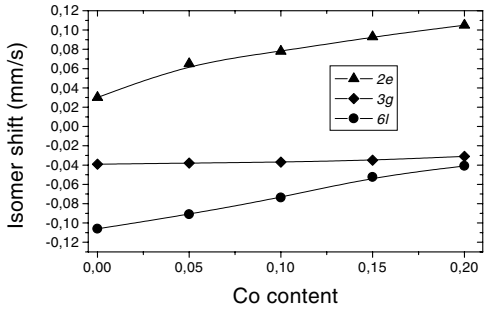

Figure 2. The compositional dependence of the isomer shifts at 293 K for hexagonal $P6/mmm$ $SmTi(Fe_{1-x}Co_x)_9$. The solid curve is a guide for eyes.

Assuming independence of the atom distribution between the various coordination shells, the total probability of the configuration α_i is $P_\alpha = \prod_{i=1}^{2} P_{\alpha_i}$, with α being the combined configuration $\alpha = \{\alpha_1, \alpha_2\}$.

P_α is then the total probability relative to the titanium and cobalt distribution respectively in the sites $6\ell (i = 1)$ and 3g $(i = 2)$.

The assertion concerning the cobalt distribution will be justified below when we discuss the coherency of the hyperfine parameter evolution versus x. Throughout the fitting process, these abundances were maintained as fixed parameters; they were normalized after those below 1.8 % had been neglected. All other parameters (δ, H_{HF}, and 2ϵ) were free. In the second step of the refinement, the deduced averaged isomer shift values were assigned to each site of the 2e, 3g, 6ℓ families according to their respective WSC volume sequence. Finally, in the last step of the fit, all hyperfine parameters were free.

The assumption relating to the titanium distribution over the 6ℓ site is supported by the relationship between tetragonal and hexagonal structures, as shown in table 1. Moreover, this assertion is corroborated in the last step of the fit when all parameters are left free. The fitted abundance value A is found to be equal to 15.6% for the 2e site, which is close to the calculated value 16.0%. This result confirms the assertion that titanium is located exclusively at 6ℓ sites.

The solid curves shown in figure 1 are the results of the fits with the constraints described above and the resulting hyperfine parameters are given, as an example for $x = 0$, in table 4.

Figure 2 shows the isomer shift evolution versus x at room temperature for the different sites. For a given x, the sequence observed is 2e $>$ 3g $> 6\ell$, as assumed from the WSC volume correlation. There is an increase for the mean isomer shift of the 2e and 6ℓ atoms upon cobalt substitution, while for the 3g atoms it remains quasi-constant. This result can be understood in terms of the preferential cobalt atom occupation. The WSC volume reduction which might contribute to an increase in the s-electron density at the iron nuclei is widely balanced by the enhancement of the d-electron density brought about by cobalt which, in turn, gives rise to a reduction of the s-electron density at the iron nuclei. The additional cobalt d electron favours the shielding of the 4s electrons. It results in an increase in the isomer shift for the iron nuclei having cobalt as first neighbours and no effect for the nuclei that belong to the sites where cobalt is located. The 2e and 6ℓ iron sites have six adjacent 3g neighbours while the 3g site atoms have only four. The 3g atoms with the fewest 3g neighbours are the least affected by the cobalt substitution and their charge density s is then not modified. Weak change is observed for the $\delta\{3g\}$. This specific 3g site behaviour then corroborates the preferential occupation of cobalt atoms at this site.

From the evolution of the 3g and 6ℓ isomer shifts versus cobalt content, we can deduce a possible crossover for x higher than 0.2. This behaviour indicates an eventual cobalt migration toward 6ℓ sites.

Table 4. Mössbauer hyperfine parameters for $SmTiFe_9$ at room temperature: hyperfine field, H_{HF} (kOe); isomer shift, δ (mm s^{-1}); quadrupole interaction, 2ε (mm s^{-1}); and relative area, A (%).

	$2e_1$	$2e_{30}$	$2e_{31}$	$2e_{32}$	$2e_{33}$	$\langle 2e \rangle$	$3g_0$	$3g_1$	$3g_2$	$3g_3$	$\langle 3g \rangle$	$6\ell_0$	$6\ell_1$	$6\ell_2$	$\langle 6\ell \rangle$
H_{HF}	250	300	279	270	260	269	235	219	210	192	220	257	246	230	251
δ	0.016	0.051	0.038	0.032	0.053	0.030	−0.022	−0.039	−0.048	−0.059	−0.039	−0.102	−0.109	−0.119	−0.106
2ε	0.052	0.015	0.063	0.017	0.048		0.043	0.032	0.027	0.016		0.025	0.035	0.032	
A	4.2	1.8	4.1	3.9	2.0	16.0	15.4	23.9	13.6	3.5	56.4	14.3	11.1	2.0	27.4

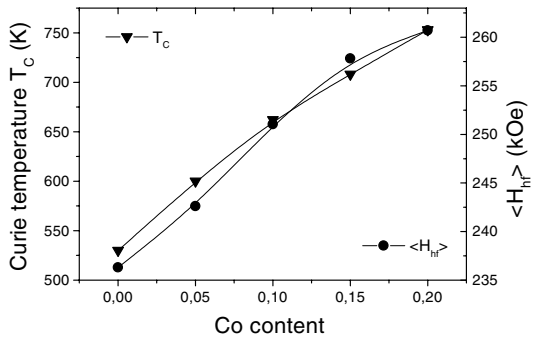

Figure 3. The Curie temperature and the weighted average hyperfine field of the partially disordered hexagonal $P6/mmm$ structure.

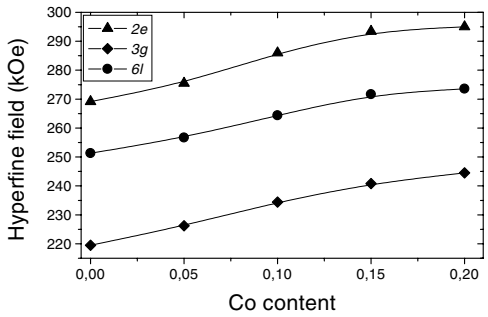

Figure 4. The compositional dependence of the hyperfine fields at 293 K for hexagonal $P6/mmm$ $SmTi(Fe_{1-x}Co_x)_9$. The solid curve is a guide for the eyes.

The mean hyperfine field increases with cobalt content (figure 3). This behaviour can be correlated directly with the mean magnetic moment variation, upon cobalt substitution, explained on the basis of a rigid-band model [20]. The increase in 3d-electron number brought about by cobalt asymmetrically fills up the 3d subbands, in conformity with the Curie temperature evolution (figure 3).

From figure 4, it can be seen that the 2e site with $11.32 - 6x$ iron neighbours shows the highest hyperfine field. This observation is in conformity with the relationship between the 1:10 precursor and its equilibrium limit 1:12 for which the recurrent 8i site shows the highest hyperfine field [21]. The 6ℓ site with $9.44-6x$ iron neighbours and $6x$ cobalt neighbours shows intermediate fields. The 3g sites with $8.88 - 4x$ iron neighbours and $4x$ cobalt neighbours has the smallest H_{HF}. The additional cobalt electron in the 3d band enhances the core electron polarization part of the Fermi contact term, the main contribution to the hyperfine field. For a given x, the 6ℓ atoms, with higher probability of having cobalt neighbours than 3g, will show higher field values. This result contrasts with that for the 1:12 structure for which the derived families 8f (formerly 3g) and 8j (formerly 3g and 6ℓ) obey the following sequence: $H_{HF}\{8f\} > H_{HF}\{8j\}$. In this last case, a more pronounced compensation for 8j than for 8f sites of the negative contribution of the core electron polarization field by the positive conduction 4s-electron polarization field can be invoked.

4. Conclusions

In this paper, we have studied the metastable $P6/mmm$ phase formation and its transformation towards the equilibrium limit $I4/mmm$. A specific code for the WSC calculation of the disordered structure has been used. The partial occupation of titanium and the partial substitution of samarium for iron–iron dumb-bells are simulated in a $P6/mmm$ subgroup.

The assignment of the various sextets to the three nonequivalent crystallographic iron sites in SmTi(Fe, Co)$_9$ is based on the isomer shifts, the sequence of which agrees with the WSC volume sequence for the three iron sites. In the SmTi(Fe$_{1-x}$Co$_x$)$_9$ alloys, upon Co substitution, the $\delta\{2e\}$ and $\delta\{6\ell\}$ increase is explained by the perturbation brought about by Co neighbours. The reduction of the s-electron density at the corresponding Fe nuclei is due to the shielding of the 4s electrons by the additional cobalt d electrons. For the 3g sites with fewer cobalt neighbours, the isomer shift remains quasi-constant which implies the location of cobalt in 3g sites.

Moreover, the evolution of the hyperfine field of the SmTi(Fe$_{1-x}$Co$_x$)$_9$ compounds, where x ranges between 0 and 0.2, clearly indicates that the hyperfine field at the iron site increases with the cobalt content, whatever the site. The hyperfine fields found for the three iron sites are very reasonable, whatever the x content, and correlate well with the number of iron near neighbours of a specific site.

References

[1] Ohashi K, Tawara Y, Osugi R and Shimas M 1988 *J. Appl. Phys.* **64** 5714
[2] Coey J M D and Sun H 1990 *J. Magn. Magn. Mater.* **87** L251
[3] Ray A E 1966 *Acta Crystallogr.* **21** 426
[4] Buschow K H J 1966 *J. Less-Common Met.* **11** 204
[5] Cadieu F J, Cheung T D, Aly S H and Wickramasekara L 1982 *J. Appl. Phys.* **53** 8338
[6] Cadieu F J, Cheung T D, Wickramasekara L and Aly S H 1984 *J. Appl. Phys.* **55** 2611
[7] Katter M, Wecker J and Schultz L 1991 *J. Appl. Phys.* **70** 3188
[8] Djéga-Mariadassou C and Bessais L 2000 *J. Magn. Magn. Mater.* **210** 81
[9] Teresiak A *et al* 1998 *J. Alloys Compounds* **217** 284
[10] Li H S *et al* 1994 *Solid State Commun.* **90** 487
[11] Ohashi K *et al* 1987 *IEEE Trans. Magn.* **23** 3101
[12] de Mooij D B and Buschow K 1988 *J. Less-Common Met.* **136** 207
[13] Rodríguez-Carvajal J, Fernandez-Diaz M T and Martinez J L 1991 *J. Phys.: Condens. Matter* **3** 3215
[14] Rodríguez-Carvajal J 1993 *Physica* B **192** 55
[15] Rietveld H M 1967 *Acta Crystallogr.* **22** 151
[16] Rietveld H M 1969 *J. Appl. Crystallogr.* **2** 65
[17] Givord D, Laforest J, Schweizer J and Tasset F 1979 *J. Appl. Phys.* **50** 2008
[18] Koch E and Fischer W 1996 *Z. Kristallogr.* **211** 251
[19] Pettifor D G 1988 *Physica* B **149** 3
[20] van Diepen A and Buschow K 1972 *J. Appl. Phys.* **43** 645
[21] Qi Q, Hu B P and Coey J M 1994 *J. Appl. Phys.* **75** 6235